International Journal of Remote Sensing

ISSN: (Print) (Online) Journal homepage: www.tandfonline.com/journals/tres20

Statistical moments of VIIRS night-time lights

Christopher D. Elvidge, Feng Chi Hsu, Mikhail Zhizhin, Tilottama Ghosh & Tamara Sparks

To cite this article: Christopher D. Elvidge, Feng Chi Hsu, Mikhail Zhizhin, Tilottama Ghosh & Tamara Sparks (2024) Statistical moments of VIIRS night-time lights, International Journal of Remote Sensing, 45:21, 7778-7802, DOI: 10.1080/01431161.2022.2161857

To link to this article: https://doi.org/10.1080/01431161.2022.2161857

Published online: 05 Jan 2023.

INTERNATIONAL JOURNAL OF REMOTE SENSING
2024, VOL. 45, NO. 21, 7778–7802
https://doi.org/10.1080/01431161.2022.2161857

Taylor & Francis
Taylor & Francis Group

Statistical moments of VIIRS night-time lights

Christopher D. Elvidge[a], Feng Chi Hsu[b], Mikhail Zhizhin[a,c], Tilottama Ghosh[a] and Tamara Sparks[a]

[a]Earth Observation Group, Colorado School of Mines, Golden, Colorado, USA; [b]Computer Science Center, National Renewable Energy Laboratory, Golden, Colorado, USA; [c]Space Dynamics and Mathematical Information Processing, Space Resarch Institute, Russian Academy of Sciences, Moscow, Russia

ABSTRACT

Annual VIIRS global night-time lights traditionally report mean radiance levels after filtering to remove moonlit and cloudy data followed by outlier removal. The mean is the first statistical moment, but there are three other statistical moments (variance, skew and kurtosis) that are currently not produced globally. In this study, we generated VIIRS day/night band multiyear and annual statistical moments for a widely dispersed set of test areas. The moments were calculated from 15 arc second nightly temporal profiles spanning 2012–2020, filtered to exclude cloudy and sunlit data, with radiance adjustments to reduce view angle and lunar illuminance effects. The moment data were examined in two ways: (1) Geospatial grids-which reveal zonation and temporal changes present in urban areas and (2) Scattergrams of moment pairs. The variance versus mean scattergram exhibits several distinct data clusters used to define five zones: core lighting, dark-erratics, mid-erratics, bright-erratics and bright and seteady. The results indicate that the information content of VIIRS night-time lights can be augmented if all four statistical moments are calculated.

KEYWORDS

VIIRS; day–night band; DNB; night-time lights; urban mapping

1. Introduction

The Earth Observation Group (EOG) has produced monthly and annual global cloud-free composites of satellite observed night-time lights data products spanning 1992 to 2021 from low-light imaging data collected by the U.S. Air Force Defense Meteorological Satellite Program (DMSP) Operational Linescan System (OLS) and the NASA/NOAA Visible Infrared Imaging Radiometer Suite (VIIRS) (Elvidge et al., 2022a). The standard product suite (Figure 1) includes 15 or 30 arc second grids tallying the total number of moonlight-free night-time observations, tally of cloud-free observations, raw average brightness (radiance for VIIRS and digital number for DMSP), outlier removed average brightness and a masked average brightness. The final product has the average brightness of lights present at the Earth's surface – with values in background areas – with no detectable lighting – set to zero. Statistical science defines four unique indices to describe

CONTACT Christopher D. Elvidge celvidge@mines.edu Earth Observation Group, Colorado School of Mines, Golden, Colorado, USA

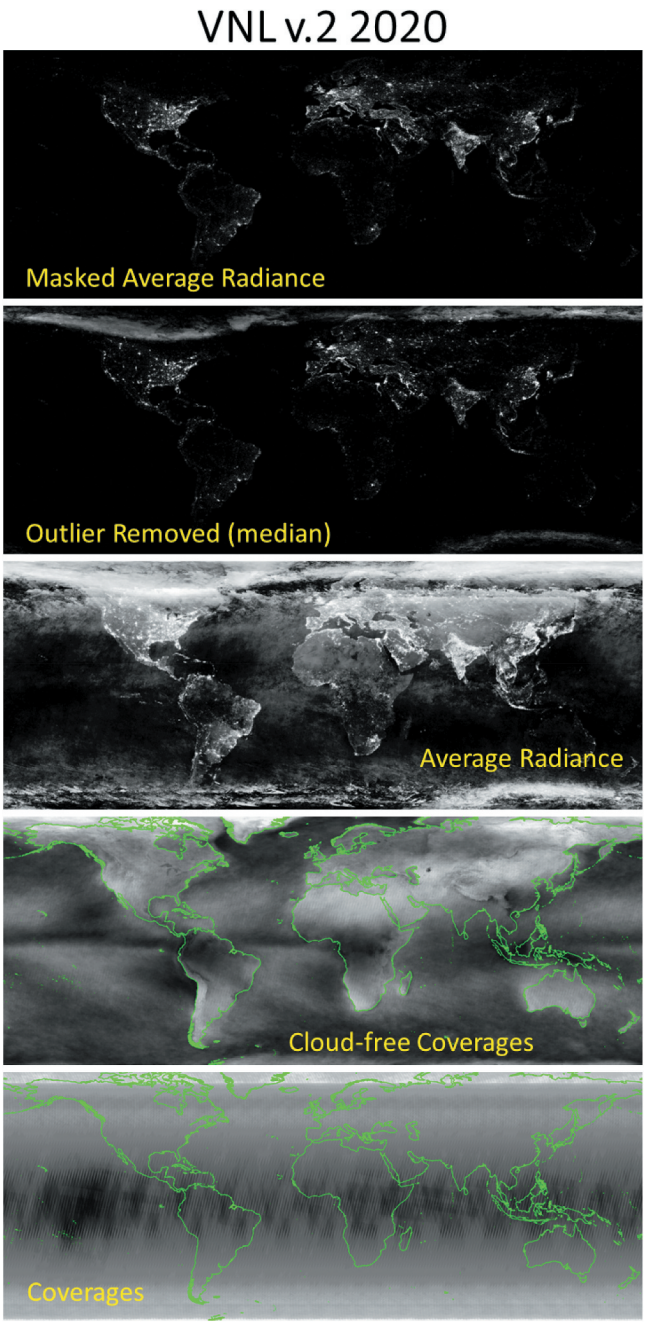

Figure 1. Basic set of annual grids from VIIRS night-time lights.

the variations in the distribution of values within data assemblages, known as moments (Krishnamoorthy 2006). As defined for the the physical sciences, the first moment is the centre-of-mass and the second moment is the object's inertia. For numerical samples, the first moment is the mean (comparable to the centre-of-mass), the second moment is variance, the third moment is skew and the fourth moment is kurtosis.

All previous global monthly and annual night-time lights products have focused on the average brightness of lights (Elvidge et al. 1997, 2017; Ghosh et al. 2021). Recent studies indicate that there is substantial information content on lighting differences present in the VIIRS DNB temporal profiles (VNL v.3) that is lost in the averaging process (Elvidge et al. 2020a, 2022b). For instance, grid cells can have nearly the same mean – yet are quite distinct from each other in the other moments. An example of this is presented in Figures 2 and 3. The samples come from a residential area in Houston, Texas (USA) and a government building in Pyongyang, Democratic People's Republic of Korea (DPRK). The temporal profiles (Figure 2) show cloud-free radiances with adjustment made to remove view angle effects and lunar reflectance (Elvidge et al. 2020a). Both have mean radiances slightly over 27 nW/cm^2/sr. The histograms of the two grid cells are quite different, with the Houston sample showing a normal distribution and the Pyongyang samples showing a highly skewed distribution with high variance and high dispersion (variance/mean).

In this paper, we explore the statistical moments of VIIRS night-time lights. The primary motivation of the study is to assess whether there are classes of lit grid cells that can only be identified with multiple statistical moments.

2. Methods

Nightly DNB temporal profiles were generated for 11,347,203 fifteen arc second grid cells from more than 60 major urban test areas and three spatially extended zones having

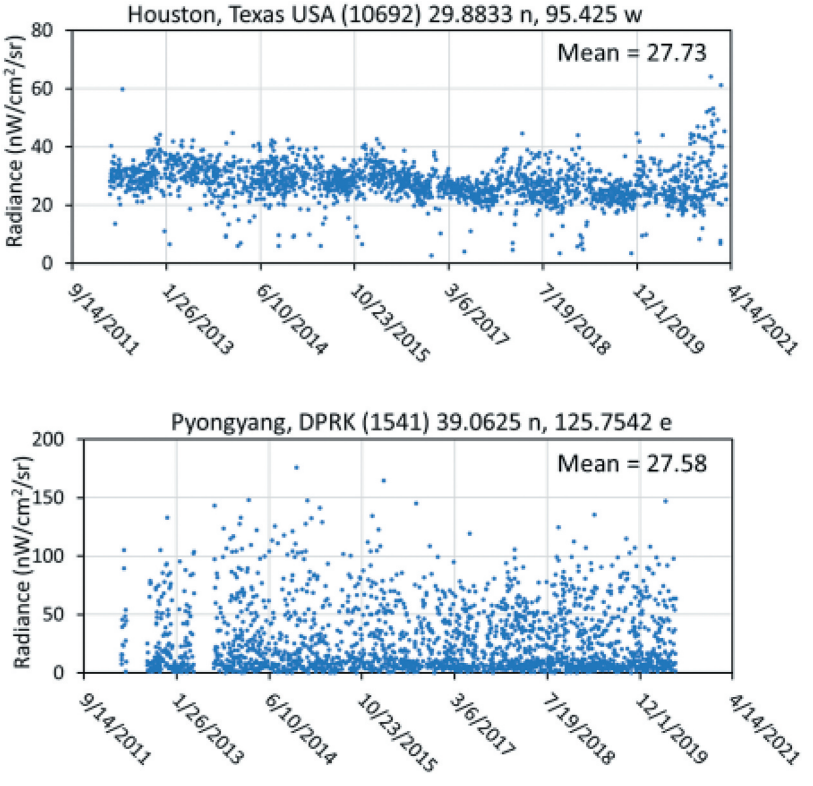

Figure 2. VIIRS DNB radiance profiles for two grid cells having nearly the same mean.

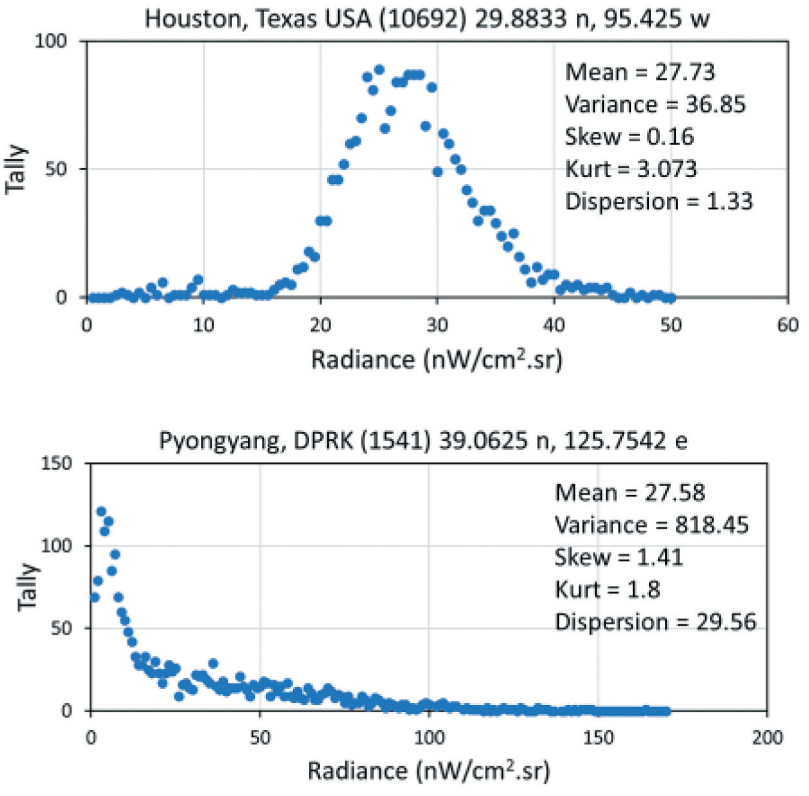

Figure 3. VIIRS DNB radiance histograms for two grid cells having nearly the same mean. The Houston sample has near a normal distribution while the Pyongyang sample is highly skewed.

many smaller human settlements and extensive background areas having no detected lighting. The locations of these test areas are shown in Figure 4. The procedures used to assemble the profiles are described in Elvidge et al. (2020a). This includes filtering to remove cloudy and sunlit data, a radiance adjustment for satellite zenith angle effects and the subtraction of the lunar radiance component. These temporal profiles form the initial core of VIIRS Nighttime Lights v.3 (VNL v.3), which EOG plans to expand over time to cover more lighting areas.

Then annual and multiyear statistical moments were calculated for grid cell. Instead of kurtosis – kurt or excess kurtosis was calculated profile and for each year. This is referred to as Pearson's kurtosis (Fiori and Zenga 2009). Annual and multiyear moment grids were produced for each of the study areas.

The grid cells were sorted to exclude background areas that lacked detectable lighting or are extremely dim. Lit grid cells were defined as those having multiyear mean radiance values of two nanowatts/cm^2/sr or more. A total of 3,984,050 lit grid cells are included in the study.

Annual and mutliyear scattergrams were generated for each test site and a merged set of all lit grid cells: (1) variance versus mean, (2) skew versus kurt, (3) skew versus mean and (4) kurt versus mean. Distinctive zones were identified from the variance versus mean

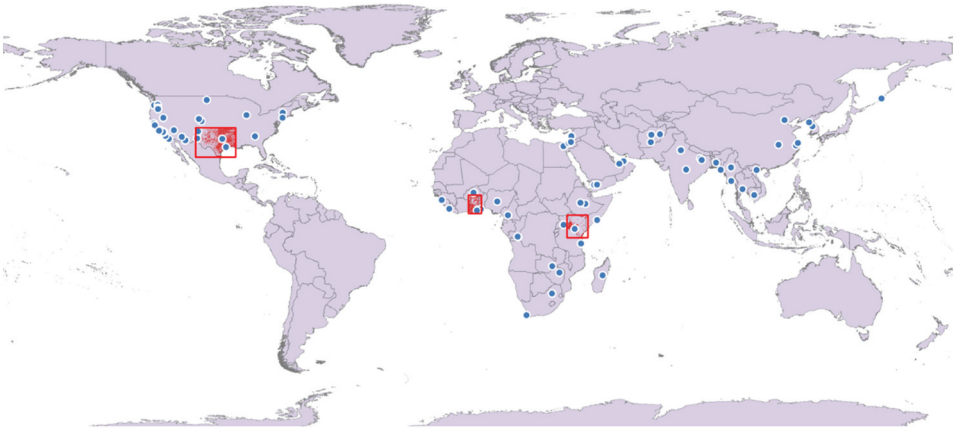

Figure 4. Map showing the distribution of DNB temporal profiles used in this study.

scattergram, exemplar grid cells were identified for each zone. Finally, colorized maps of the zones were produced – showing internal structures with urban centres.

Scattergrams were generated for variance versus mean, skew versus kurtosis, skew vs mean and kurtosis vs mean. These were visually inspected and then representative grid cell samples were selected as exemplars for specific zones found in the variance versus mean scattergram.

3. Results

3.1. Moment grids

Annual and multiyear 15 arc second grids of the four moments were produced for each of the test areas shown in Figure 4. The moment grids are suitable for analysing zonation patterns within lit areas and the evolution of night-time lights from 2012 to present and are available on an open access basis.

Figure 5 shows moment grids from 2020 for two distinctly different urban centers: Delhi, India and Houston, Texas. The lighting in Delhi is relatively dim compared to Houston and has fewer pockets of bright lighting. Houston exhibits a hub and spoke pattern (O'Kelley, 2009), where residential areas are dimmer and commercial areas and major roadways are brighter and have great variance. Lit areas tend to have both lower skew and kurtosis. This is particularly pronounced in Houston.

Figure 6 shows annual moment difference images with the 2020 minus 2013. The grid cells having multiyear means less than 2 nW are masked to zero. A large portion of central Delhi had a decline in both the mean and variance going from 2013 to 2020. This is an indicator for the conversion of high-intensity discharge (high-pressure sodium and metal halide) to LED streetlights (Elvidge et al. 2022b). Houston exhibits increases in the mean in the outskirts and patches of dimming in the central area. There are distinct zones of decreased variance in Houston – which may be an indicator of LED conversions. There is a slight decline in skew in the central part of Delhi, with a mixed pattern of increased and decreased skew in the outskirts of Delhi. Houston exhibts a decline in skew in the north and

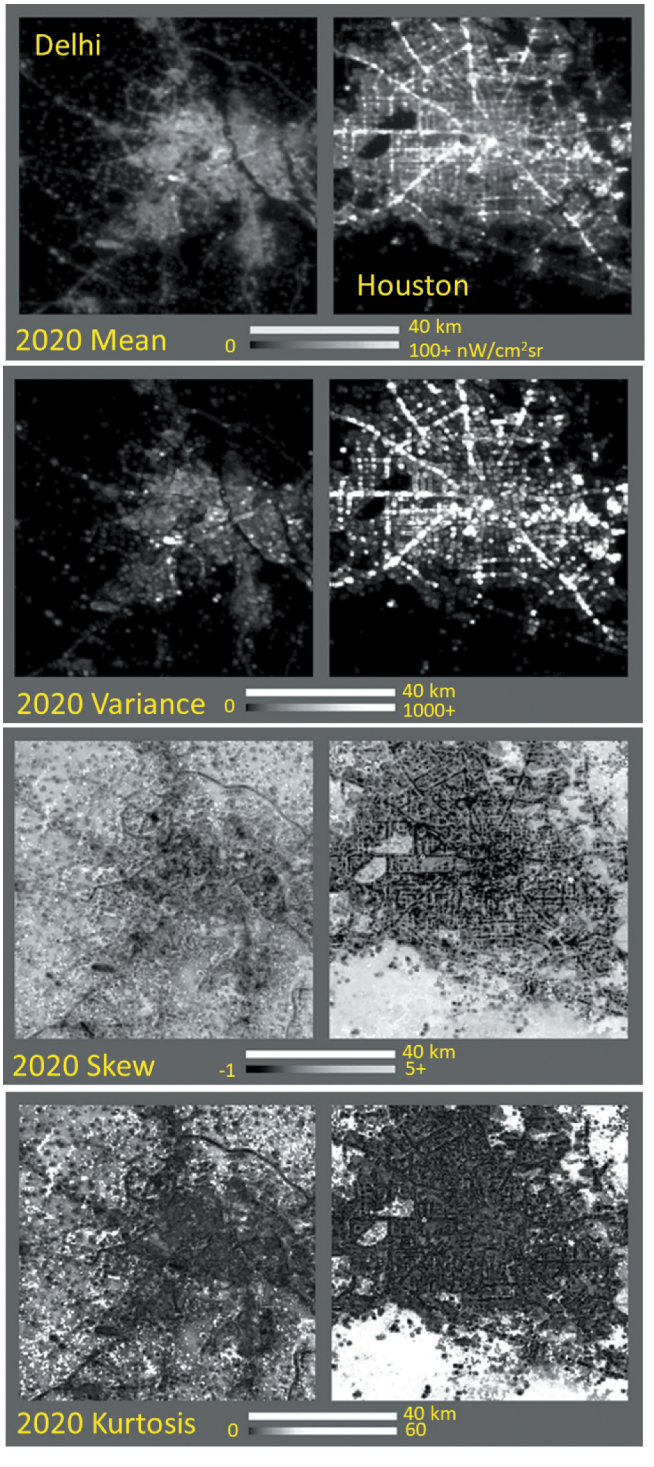

Figure 5. Fifteen arc second annual moment grids for Delhi, India, and Houston, Texas, from the year 2020.

western sections of the city. The central sections of Delhi and Houston were largely stable in kurtosis from 2013 to 2020. Zones with increased or decreased kurtosis are on the outskirts.

3.2. Overview of moment scattergrams

By pooling all lit grid cells from the test sites (Figure 4) it is possible to explore the features present in VNL statistical moments via scattergrams formed with key moment pairs (Figure 7). The central scattergram has the first and second moments, mean and variance, shown in Figure 7a, with variance on the x-axis and mean on the y-axis. The scattergram scaling is from 0 to 400 nW for the mean and 0 to 12,000 for variance. This scaling covers more than 99% of the grid cells – though there are small numbers of grid cells that exceed the axis ranges. The variance versus mean scattergram has three unique features. First, there is a dense core of grid cells having dim to moderately bright radiance and relatively low variance. Second, there is a spur formed by grid cells where the mean is relatively low and variance is high. And third is a zone having a wide range of mean radiances and extremely high variance.

The scattergram for the third (skew) and fourth (kurt) moments is presented in Figure 7b, with skew on the x-axis and kurt on the y-axis. Here the grid cells form a compact swoosh pattern, indicating that the two moments are highly correlated. Skew can be either positive or negative and ranges from negative 2 to 15. Kurt spans from 0 to 230. The skew versus kurt data cloud has a parabolic shape, with a vertex set near a skew of zero, defining the axis of symmetry for the data cloud. The tail of the parabola is substantially longer on the positive skew side, with kurt values increasing – forming and tight bond to increased skew. The parabola tail is much shorter on the negative skew side, with kurt increasing in synchronization with the decline in skew.

The scattergram for the third and first moments (skew vs mean) is shown in Figure 7c. The data cloud shows a symmetrical cone for mean radiances above 60 nW and a long tapered tail extending towards high skew values for mean values between 2 and 60 nW.

The fourth key scattergram, Figure 7d shows the first and fourth (kurt vs mean) moments on the y and x-axis, respectively. Here, the data cloud forms an 'L'-shaped pattern with a right angle vertex near the origin. The vertical axis of the 'L' has widely variable mean values and low kurt. The horizontal axis has grid cells with low mean radiances and widely varying kurt.

3.3. Examination of the variance versus mean scattergram

Of the four scattergrams presented in Figure 7, the variance versus mean has the greatest expression of zonation, which offers the possibility of dividing the data cloud into a set of distinct zones. We decided to examine this scattergram more closely and discovered that the mean is related to the square root of variance for two of the zones. The lower spur, having low means and high variance, can be separated from the upper variance lobe by the fucntion $y = 0.75\text{sqrt}(x)$. The upper lobe, where both mean and variance are high, is bisected by the function $y = 2.5\text{sqrt}(x)$.

3.3.1. Zone of "dark erratics"

Two of the data clusters having the highest variance on the variance versus mean scattergram (Figure 8 and 9) are separated by a data density gap that can be delineated

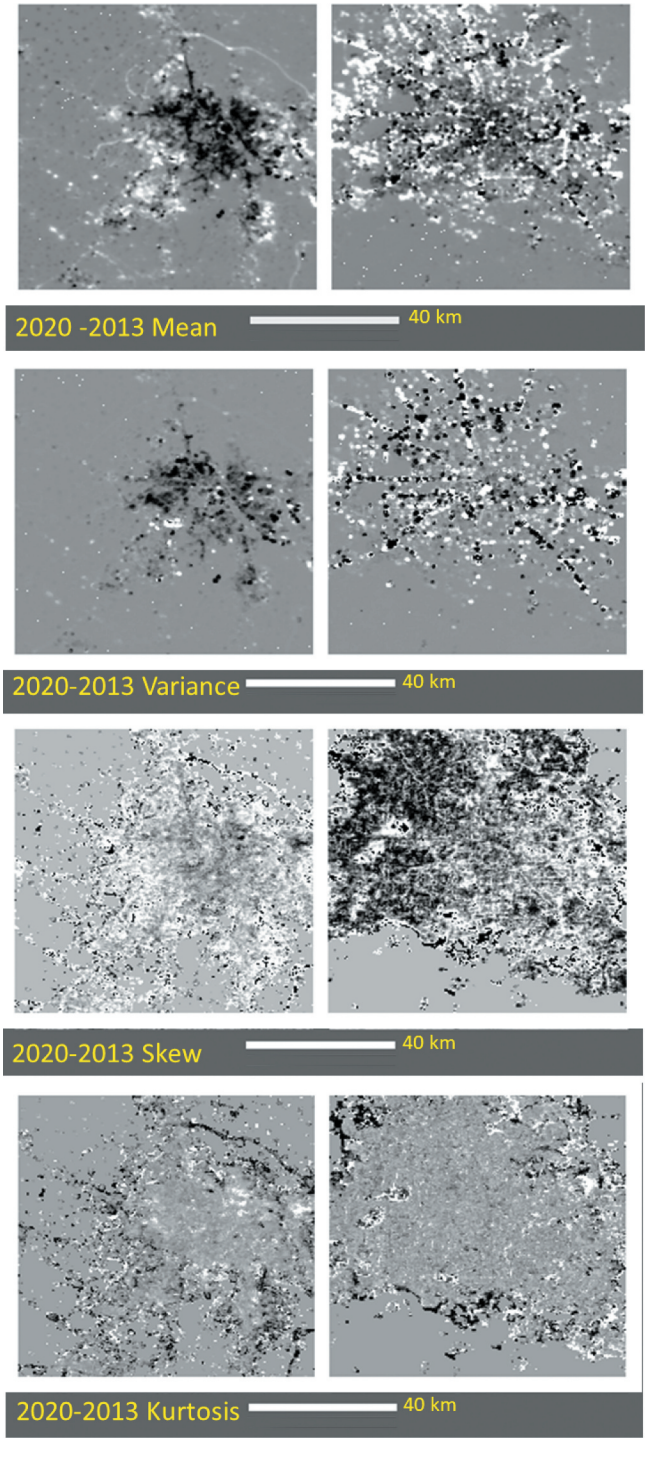

Figure 6. Moment difference images from Delhi and Houston for 2020 minus 2013.

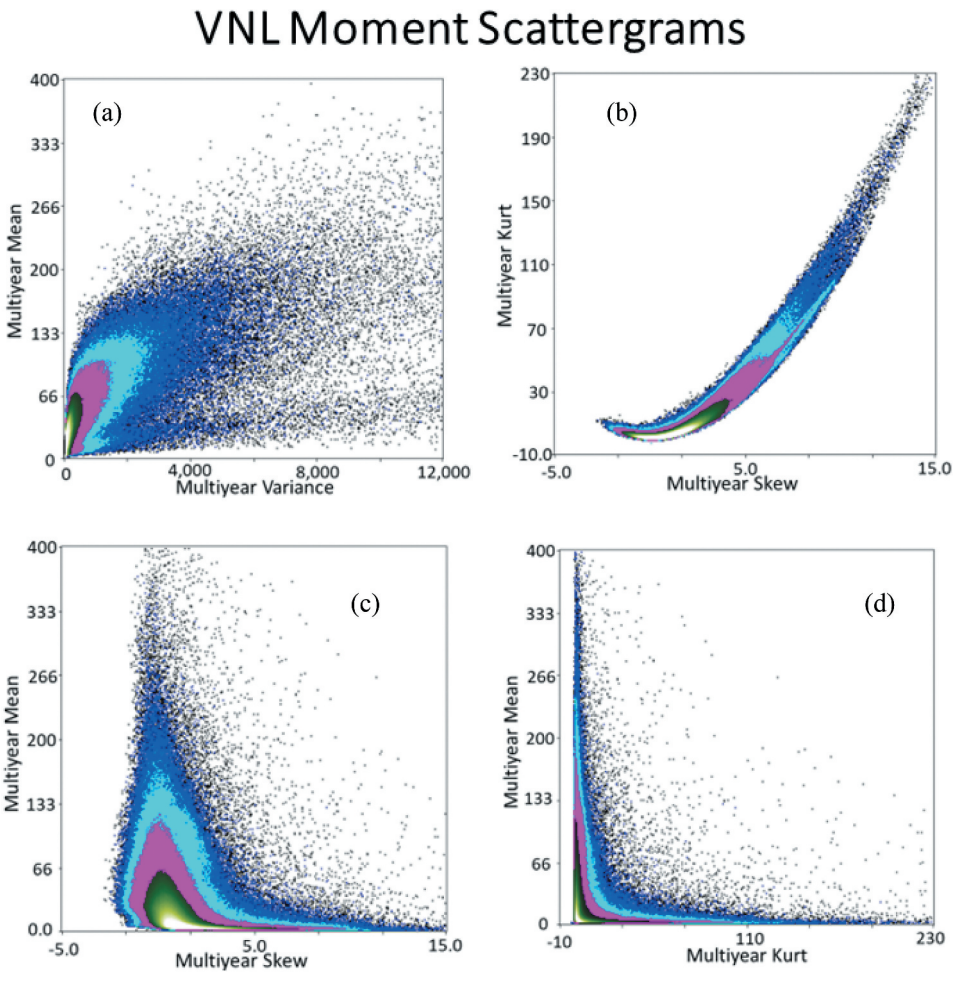

Figure 7. Four key moment scattergrams: variance versus mean in 7a, skew versus kurt 7b, skew versus mean 7c and kurt versus mean 7d. Each scattergram is formed from the multiyear moments calculated for 3,984,050 grid cells having mean lighting of 2 nW or higher.

with the function: mean = 0.75(sqrt variance). The name we have assigned to this zone below this line is the 'dark-erratics', where mean remains low and variance runs high. Temporal radiance profiles for this zone frequently drop to extremely low values, often reaching the noise floor of the sensor – near 1 nW. The low baseline radiance is periodically interrupted by nights with extremely high radiance levels. The most common source of dark-erratics are intermittent gas flares in areas having little or no surface lighting detected when the flare is not active. A dark-erratic exemplar is shown in Figure 10. This temporal profile has most of the records with extremely low radiances, with high radiances occurring intermittently. The histogram for grid cells in this zone exhibits a mode coinciding with the sensor's noise floor with long tail extending to extremely high variance levels. These grid cells have low means, but the three other moment levels are high.

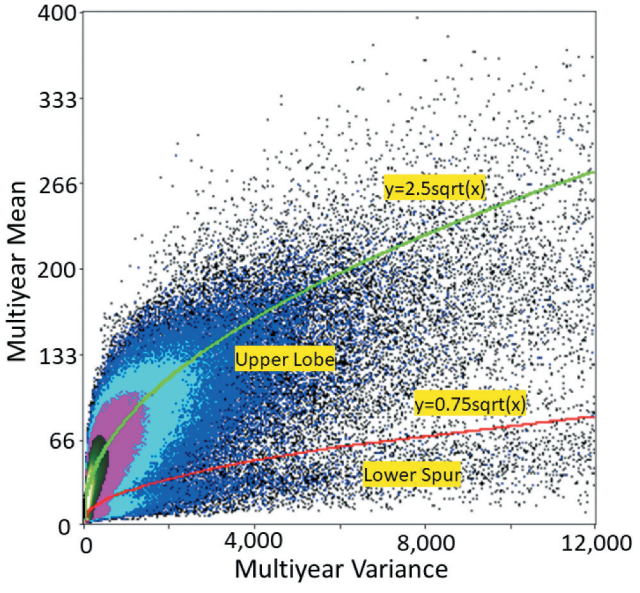

Figure 8. The zone of 'dark-erratics' is below the line formed by the function mean = 0.75*sqrt of the variance. The line y = 0.5sqrt(x) tracks the centre centre of the dark-erratic zone. The zone of 'bright-erratics' is bisected by the line formed by the mean = 2.5*sqrt of the variance. In contrast, the core lighting zone trajectory is y = 0.14(x).

3.3.2. Core lighting

The variance versus mean scattergrams for urban areas all exhibit a dense core of grid cells having modest lighting levels and moderate levels of variance. The feature appears as a near vertical column extending to the origin on the variance versus mean scattergram. The dense vertical column tilts slightly to the right on the scattergram – tracking growth in variance as the brightness of lighting increases. This is the 'core lighting' zone, which can be isolated from other zones as grid cells in this sample set with mean radiances less than 70 nw and variance levels under 560 (Figure 9). The core lighting zone contains 96% of all the lit 15 arc second grid cells from the test areas (Figure 4). The core lighting zone abuts the dark erratic zone near the scattergram origin. Close inspection of dark-erratic zone versus urban lighting reveals there is surprisingly little overlap between core lighting and dark-erratics.

An exemplar of core lighting is shown in Figure 11 – from a mixed-use urban grid cell found in Phoenix, Arizona. Another example of core lighting is the Houston grid cell shown in Figures 2 and 3. Core lighting temporal profiles exhibit a steady mean over time – and a moderate amount of variance. The histograms closely resemble a Gaussian distribution.

3.3.3. Bright erratics

The bright erratic zone is defined as grid cells having higher mean and higher variance values relative tothe core lighting zone. That is, mean values greater than 70 nW and variance levels greater than 560 (Figure 9). An exemplar of a grid cell from the bright erratic zone is shown in Figure 12, from Las Vegas, Nevada. Radiance levels are highly

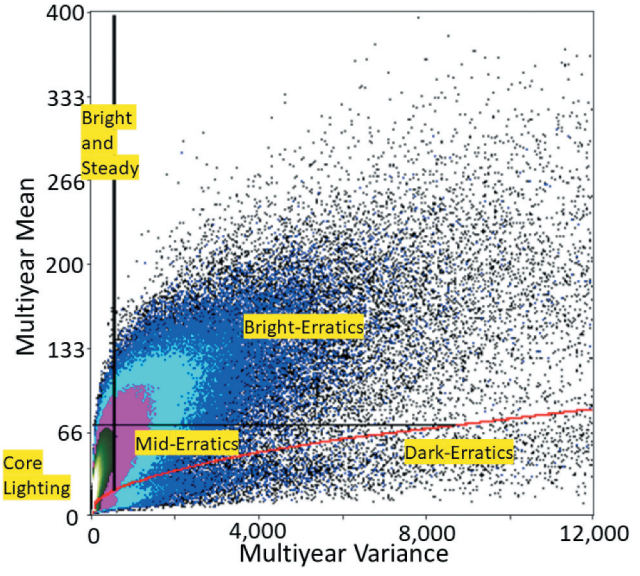

Figure 9. Five distinct zones can be identified on the variance vs mean scattergram: (1) There is a dense zone of 'core lighting' extending from near the origin and upward along the mean axis. (2) There is a spurt of 'dim erratics' spur formed by grid cells having high variance and low mean radiances. (3) The 'bright steady' zone has the same variance range as core lighting – but higher mean radiances. (4) the 'bright erratic' zone has grid cells that have higher mean and variance values than the core lighting. And (5) the 'mid-erratic' zone is defined between the core lighting, dark erratics and bright erratics.

variable in this temporal profile, frequently changing from low to high in an erratic fashion. The erratic fluctuation in brightness may trace back to alternating current flicker, common with outdoor metal halide and high-pressure sodium lighting (Elvidge et al. 2022b). The exemplar histogram (Figure 12) shows an extremely broad distribution, with high mean, high variance, low skew and low kurt.

3.3.4. Bright and steady

The bright and steady zone is defined as having mean radiance levels above that of core lighting – but comparable variance levels (Figure 8). These grid cells are relatively uncommon as the trend is for variance to be much higher than the mean for brightly lit grid cells – forming the bright-erratic zone. The bright and steady zone sits above the core lighting and to the left of the bright-erratic zone. An exemplar for the bright and steady zone is shown in Figure 13 – a grid cell dominated by urban highway lighting found in Houston, Texas. The histogram shows a largely Gaussian distribution, offset to higher mean radiance levels as compared to the core lighting. Skew and kurt are low.

3.3.5. Mid-erratics

The mid-erratic zone is defined as grid cells found in the gap between three other zones: core lighting, dark erratics and bright erratics (Figure 9). Grid cells in this zone have the same mean radiance cap as core lighting – but have higher levels of variance. This is a highly variable zone – ranging from grid cells ringing patches of

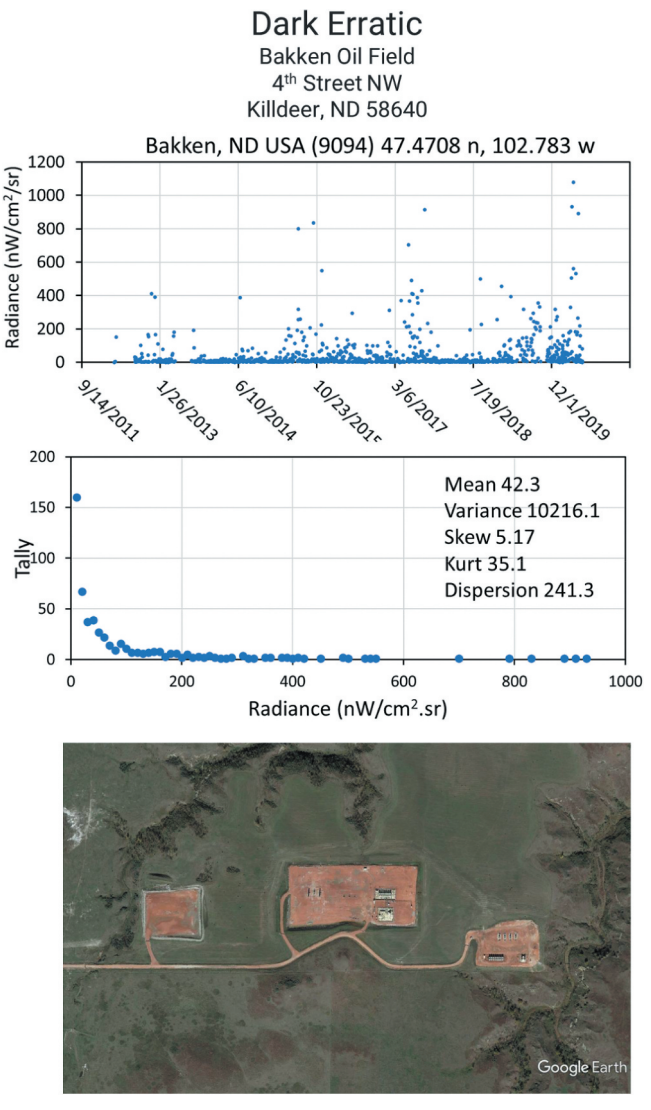

Figure 10. An exemplar of the 'dark erratic' zone from the Bakken oil field in North Dakota, USA.

bright erratics to grid cells where the light levels have fluctuated substantially over time due to conflict or frequent power generation shortfalls. The Pyongyang grid cell shown in Figures 2 and 3 is an example of a mid-erratic. An exemplar for mid-erratics is shown in Figure 14, a grid cell from the central portion of Mari'b, Yemen. The Mari'b temporal profile shows the electric power supply has been built up multiple times, interrupted by multiple periods with low levels of electric power. The city was hit by aerial bombing in March of 2015, resulting in a near-complete loss of detectable lighting. There is evidence of annual cycling and there are several higher radiance spikes corresponding to annual Ramadan festivities. Skew is positive, and kurt is low.

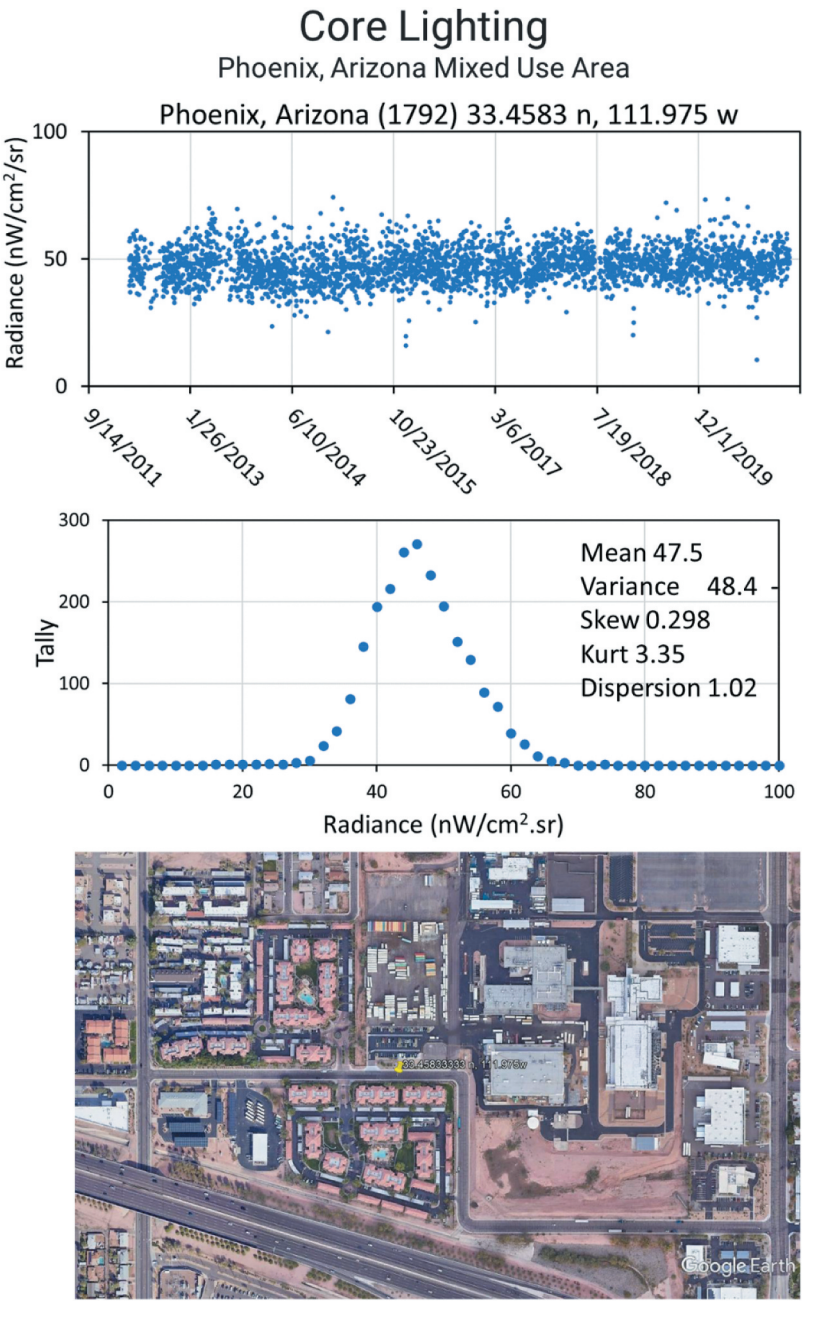

Figure 11. Exemplar of a "core lighting" grid cell from a mixed use grid cell from Phoenix, Arizona.

3.3.6. Marking the exemplar locations on the variance versus mean scattergram

Figure 15 shows the variance versus mean scattergram with the zone exemplar grid cells marked. The exemplars span the four zones defined for the scattergram: core lighting (CL), dark-erratics (DE), bright-erratics (BE) and bright and steady (BS).

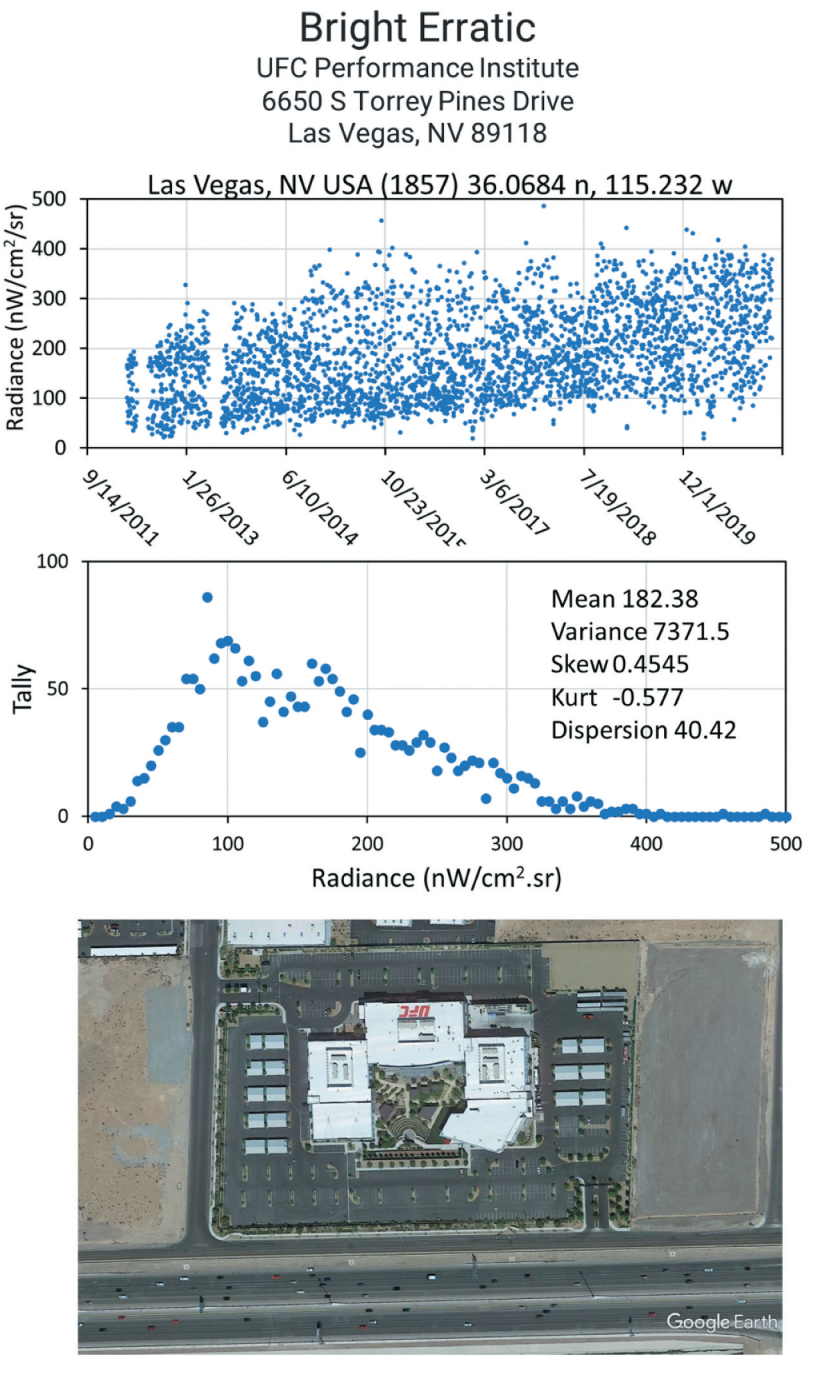

Figure 12. Exemplar for the bright erratic zone found in Las Vegas, Nevada.

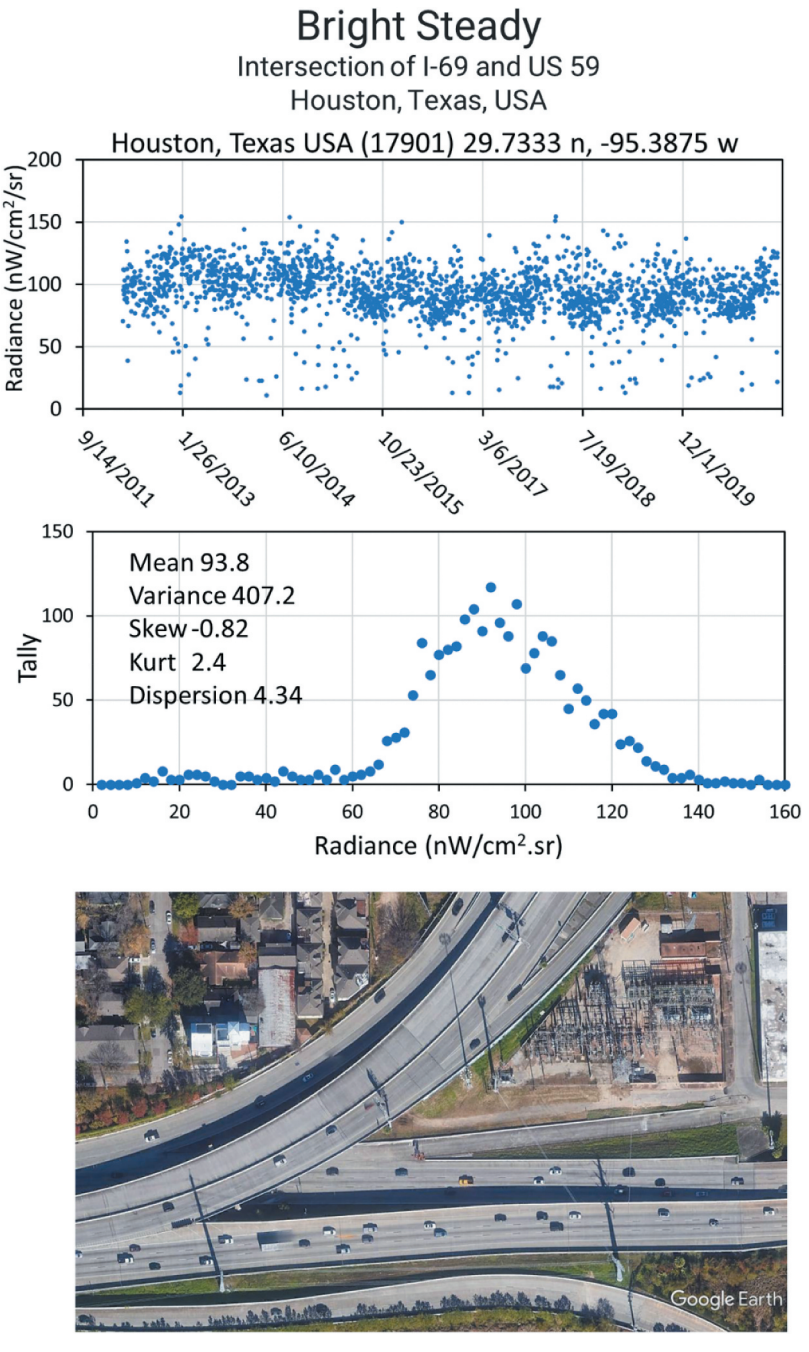

Figure 13. Exemplar of the bright and steady zone from Houston, Texas. Lighting in the grid cell is dominated by interstate highway lighting.

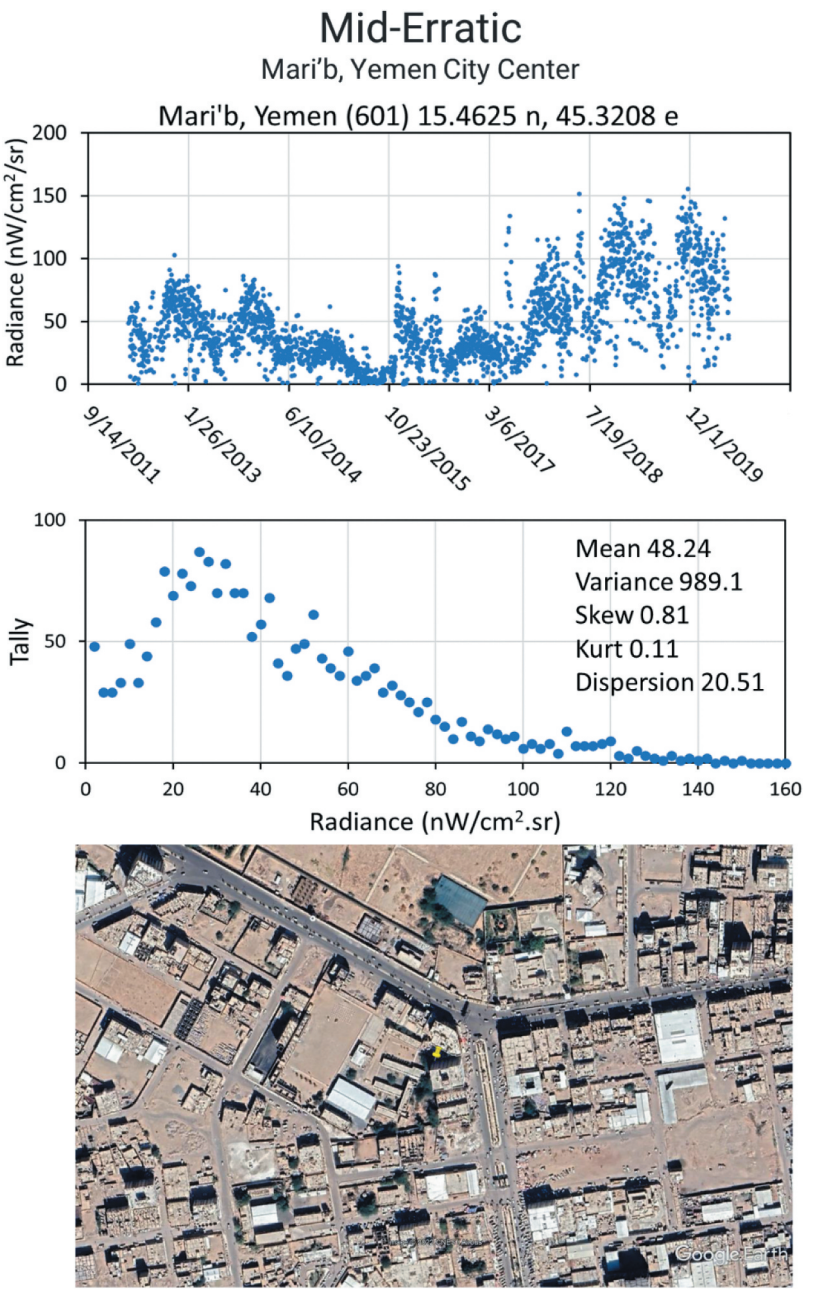

Figure 14. Exemplar of a mid-erratic grid cell from Mari'b, Yemen. The grid cell features annual cycling in the brightness of lighting and evidence of conflict induced power shortfalls, particularly from 2014 through 2017. Radiance spikes associated with Muslim holidays are present in many years.

3.3.7. Zone mapping on moment grids

It is possible to generate zone maps from the moment grids based on the variance versus mean scattergram zones. Here we take the five zones identified on variance versus mean scattergram (Figure 9) and map the zone locations on the gridded moments for Delhi and Houston. The result is shown in Figure 16. Both urban centrescentres are ringed by rural areas that either lack detectable lighting or are have multiyear mean radiances below 2 nW. They are marked dark green on the zone maps. In each case, the largest lit zone is core lighting – not surprising since this zone encompasses 96% of the lit grid cells from the combined set of test sites shown in Figure 4. Neither Delhi of Houston have grid cells falling in the dark erratic zone. However, both Delhi and Houston have grid cells from the other three zones. The largest block of bright-erratic grid cells in Delhi is the international airport – coloured red on Figure 16. In addition, there are two patches of the bright and steady zone, associated with brightly lit commercial centres – marked yellow on Figure 16. Houston has vastly more clusters of bright-erratics – corresponding to brightly lit commercial centres forming the hub and spoke pattern. In addition, there are several patches of bright and steady in the centre of town and extending to the west. Grid cells falling in the mid-erratic zone are arranged in rims around most of the red bright-erratic patches. There are several isolated bright and steady patches surrounded by core lighting.

3.4. Examining the skew versus kurtosis scattergram

One of the findings that surprised the authors is the parabolic pattern found for the skew versus kurtosis data distribution. However, this condition has been previously noted by researchers in other fields and has been described by Sattin et al. (2009). To develop some understanding of the skew versus kurtosis data distribution, we selected three grid cells for examination: high skew and high kurtosis, near-zero skew and negative skew.

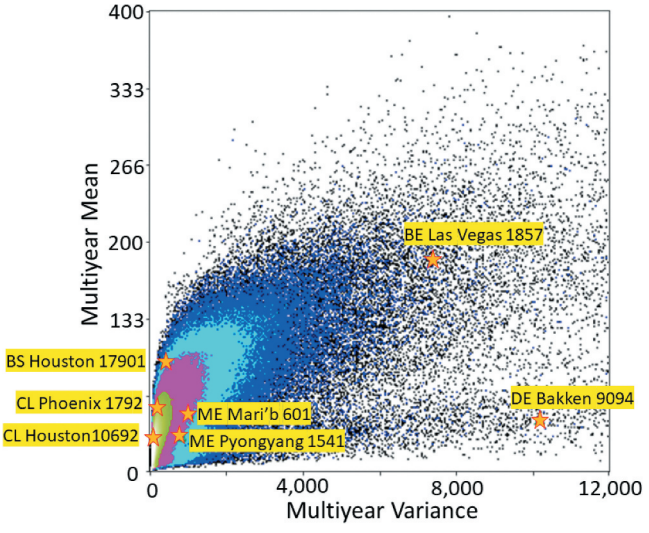

Figure 15. Location of variance versus mean exemplars on the scattergram. The prefix codes on the point labels identify the zones. DE = bright erratic. ME = mid-erratics. CL = core lighting. BS = bright and steady. BE = bright-erratic.

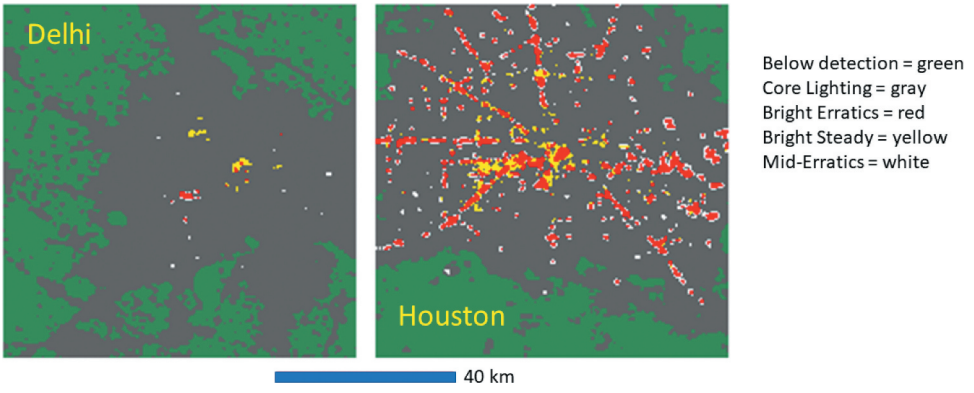

Figure 16. Colorized maps of lighting zones in Delhi and Houston based on variance versus mean divisions shown in Figure 9.

3.4.1. High skew and high kurtosis

Figure 17 shows a grid cell having both high skew and high kurtosis. The grid cell covers the Keystone Gas Processing Plant near Kermit, Texas. The temporal profile and histogram shows that the site is quite dim on most nights, yielding radiances in the 0–20 nW range. Periodically, the site has extremely high radiances, up to 1200 nW. The radiance spikes are probably the result of intermittent gas flaring. Skew is high because the data cloud is truncated by the sensor's detection limit. The intermittent radiance spikes have driven the kurtosis to over 200. This site's mean of 57 and variance of 52,144 places it in the dark-erratic zone.

3.4.2. Near-zero skew

Figure 18 shows a grid cell from near the centre of Delhi, India, having near-zero skew and low kurtosis. This particular grid cell shows annual cycling, a widespread phenomena in Northern India associated with electric power shortages (load shedding) during summer months (Hsu et al. 2021). There are upward radiance spikes that may be the result of festivals such as Diwali. There are also clusters of pixels having substantial radiance drops that may be the result of non-cyclic power shortfalls. The upward and downward radiance outliers nearly balance – resulting in a skew near-zero.

3.4.3. Negative skew

Figure 19 shows a grid cell from Houston having negative skew. The skew can be traced to the scattering of pixels with radiance drops relative to the main data cloud – in the range of 0–50 nW. There are very few upward data spikes – creating an asymmetry in the histogram – with a long tail to the left of the mean – and a negative skew. In this case, the radiance drops tend to be isolated from each other, as opposed to the clustering of low radiance pixels seen in Figure 18. While some of the low radiance night may be due to power shortfalls – another plausible explanation is that the low radiance pixels may be cloudy and have been mislabelled as clear. This is similar to the radiance drops traced to errors in cloud detection reported by Elvidge et al. (2020b).

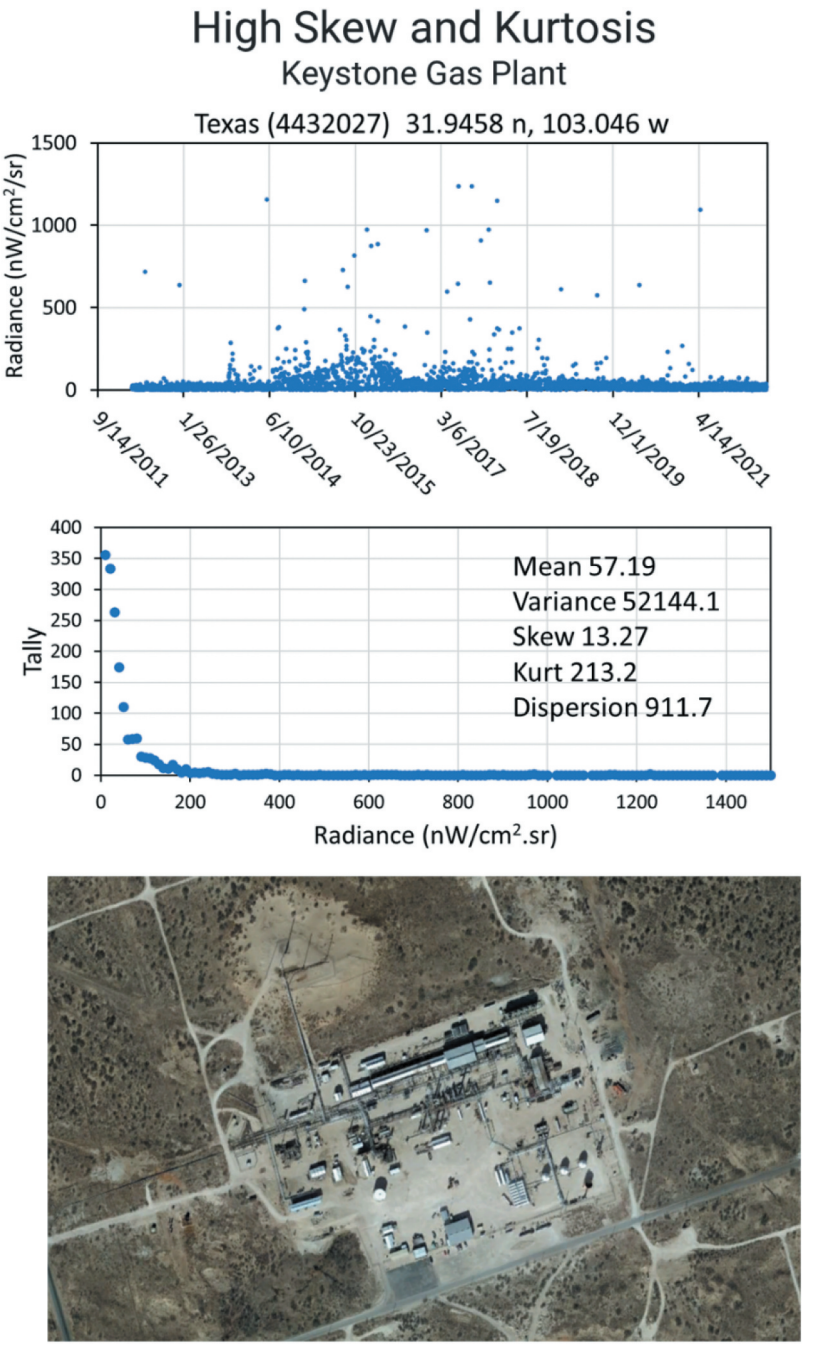

Figure 17. The Keystone Gas Processing Plant, near Kermit, Texas is an exemplar of a site having high skew and high kurtosis in VIIRS night-time lights.

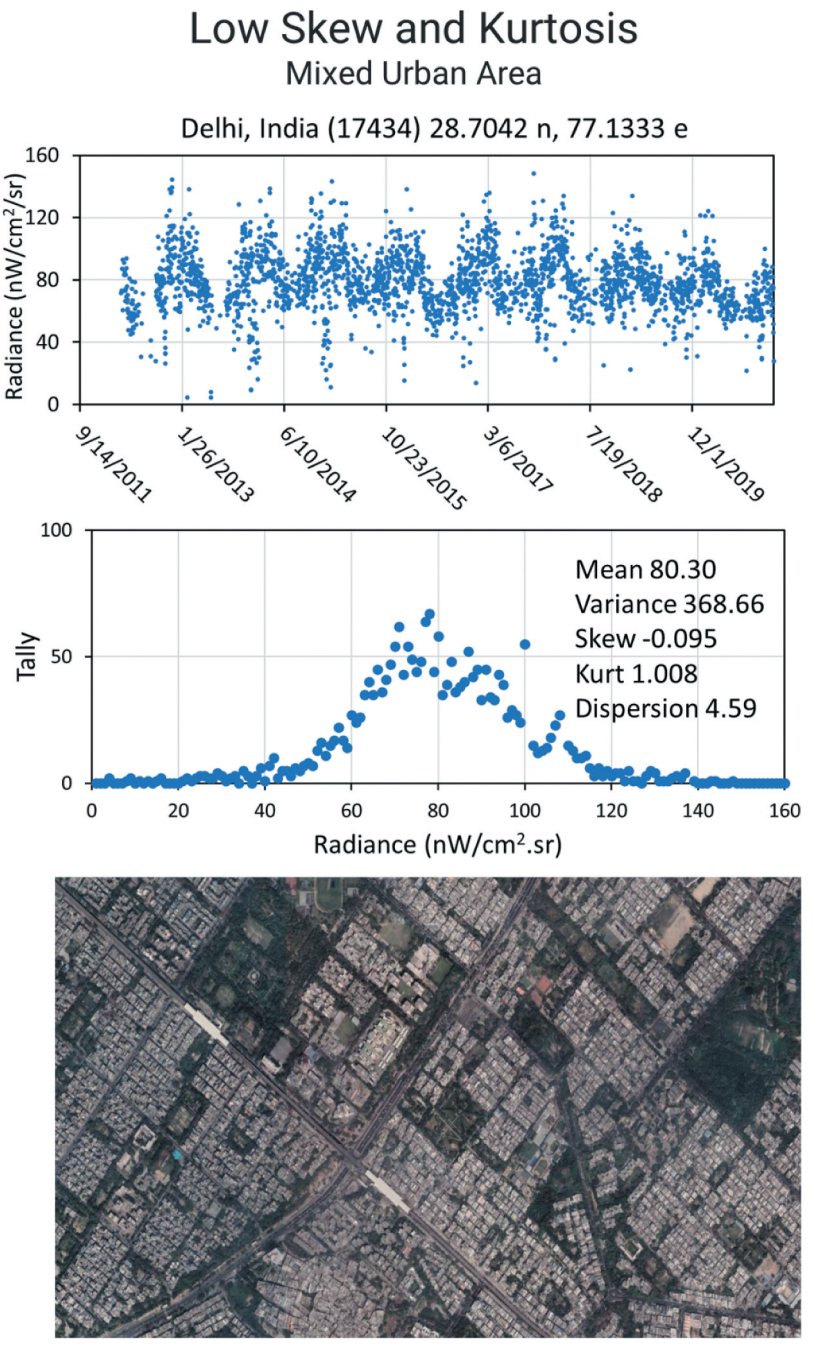

Figure 18. Grid cell from near the centre of Delhi, India, with near zero skew and low kurtosis.

3.4.4. Marking the exemplar locations on the skew versus kurtosis scattergram

Figure 20 shows the skew versus kurtosis scattergram with the placement of the Figures 17–19 exemplars marked. Detection limits and outliers play a key role in driving skew and kurtosis to extreme ranges.

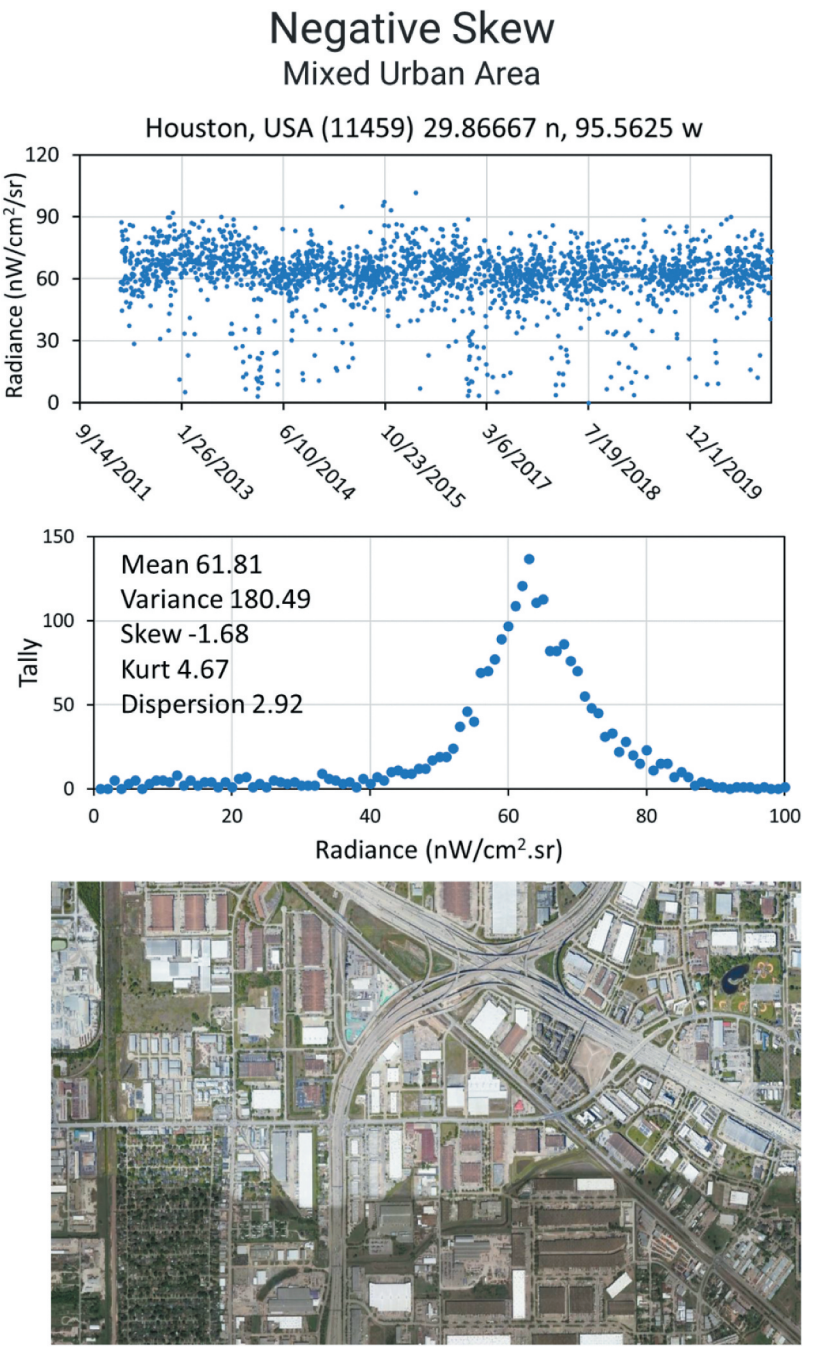

Figure 19. Grid cell having negative skew from the central part of Houston, Texas.

4. Discussion

Both skew and kurtosis exhibit detection limit effects in grid cells where the DNB radiance frequently drops to near the noise floor. This results in positive skew and often high

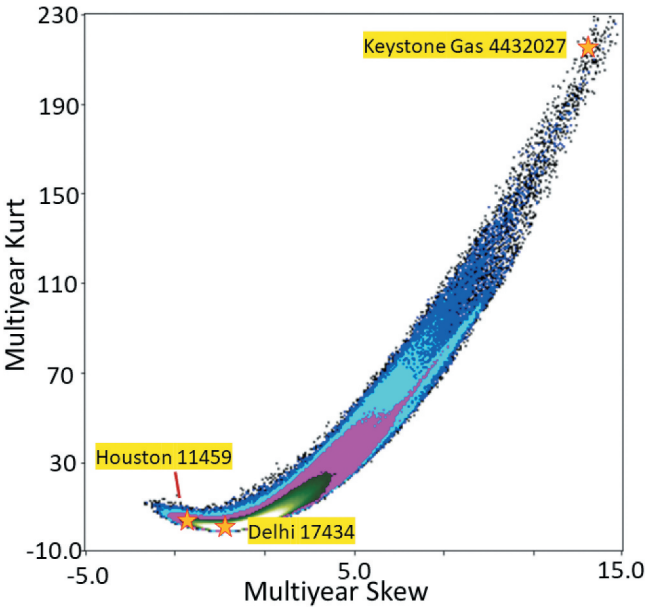

Figure 20. Placement of Figures 17–19 exemplars on the skew versus kurtosis histogram.

kurtosis. The zone most prone to detection limit effects are the dark-erratics. However, detection limit effects are also present in some grid cells from the mid-erratics (Pyongyang Figure 3 and Mari'b Figure 13) and dimly lit members of core lighting.

One of the quandries of satellite observed night-time lights is how to separate grid cells with lighting detection from background. For global products, it is impossible to set a single radiance threshold for separating dimly lit grid cells with lighting from background. This is because the background brightness varies both spatially and temporally. In general, the background brightness rises at high latitudes. This may be due to lighting from auroral events. EOG generates annual global VIIRS night-time light product sets, such as those in Figure 1 with lit grid cell masks based on data-range thresholds. Data-range is calculated as the maximum minus minimum radiance in three-by-three tiles centred on each 15 arc second grid cell. With this approach the radiance threshold for discriminating lit grid cells from background is allowed to vary. But in general, the radiance threshold is near 1 nW/cm^2/sr. For this study, we applied a uniform threshold of 2 nW, which resulted in 35% of the grid cells from Figure 4 being selected as lit. The 2 nW lighting threshold was selected based on our familiarity with the data and our desire to exclude background grid cells from the analyses. There is no single correct or definitive method discriminating lit grid cells from background. It is important to specifiy the method and to provide access to the intermediate grids, from which a research could set their own lit grid cell thresholds. EOG does exactly this, providing open access to the raw and outlier removed annual mean radiance grids, as well as the background masked average radiances and lit grid cell mask.

There is substantial variability in the core lighting zone, which contains by far the largest proportion of grid cells. It may be possible to split this zone into a set of bands having differing levels of variance.

One of the applications for the annual moment grids is to track the growth and expansion of lighting through time. Newly lit grid cells will first appear near the origin of the variance versus mean scattergram and gradually grow in brightness and variance to join one of the five zones. In fact, grid cells may pass through core lighting and the mid-erratic zone before settling in the bright erratic zone.

The position of grid cells on the scattergrams may change as a result of lighting conversion – such as the replacement of high-pressure sodium lights with LEDs. Conversion to LED lighting can result in a decrease in variance, a phenomena that has already been demonstrated (Elvidge et al. (2022b)).

5. Conclusion

For decades, global cloud-free night-time light products have only reported mean brightness levels (Elvidge et al. 2022a), the first statistical moment. This is true for both the original DMSP night-time light time series (1992–2013), the predawn DMSP extension series (2013–2021) and the VIIRS time series (2012–2021). This study makes it clear that there is substantial additional information in the other three statistical moments (variance, skew and kurtosis). Grid cells can have nearly the same mean – but exhibit sharply different values in other moments.

Variance emerges as an equal partner to the mean for characterizing the temporal behaviour of night-time lights. We identified five zones on the variance versus mean scattergram: core lighting, dark erratics, bright erratics, mid-erratics and bright and steady. Core lighting is moderately bright and has relatively low variance. Core lighting is the most ubiquitous, accounting for 96% of the lit grid cells examined in this study. DNB radiances for grid cells from the dark-erratic zone, common in areas with intermittent gas flaring, have sporadic bright spikes set on top of a stream of low radiance values. The bright-erratics have high radiances and extremely high variance and is typical in the most brightly lit commercial centres and airports. The bright and steady zone is perched above the core lighting zone on the variance versus mean scattergram. The mid-erratic zone occupies the area between the core lighting, dark-erratics and bright-erratics. Mid-erratic grid cells are found on rims surrounding patches of bright-erratics and in conflict zones where electric power supplies are fluctuating.

All of the sites examined (Figure 4) show some representation of the five variance versus mean zones delineated from the multisite scattergram (Figure 9). The dark-erratic zone is missing from the scattergrams for most individual sites. In addition, the other zones are frequently smaller and dimmer than those found with multisite scattergram. Researchers focussed on a single area should consider resetting the core lighting thresholds to more precisely match the core zone in their study area. It should also be noted that researchers may chose to develop their own set of zones or to insert subdivisions within the zones defined in this paper.

The fact that the core lighting zone is a distinct entity is demonstrated by its unique angular trajectory on the variance versus mean scattergram and the density of grid cells as compared to the other zones. The trajectory of the dark-erratic zone is $y = 0.5\text{sqrt}(x)$ and the and the bright-erratic zone's trajectory is $y = 2.5\text{sqrt}(x)$. The density of grid cells in these two zones is quite low. In contrast, the trajectory of core lighting is quite different from either of these ($y = 0.14(x)$) and the density is higher than any other part of the scattergram. As a result of the trajectory difference, the line bisecting the bright-erratics zone crosses midway through the core lighting cluster on Figure 8.

It is clear that the global annual VIIRS night-time lights time series should be reprocessed to add the other three statistical moments. The benefit with adding the other three statistical moments for the DMSP series is complicated by the data's lack of in-flight calibration and the presence of saturation on areas of bright lighting – including the cores of most urban centres. The calibration and saturation issues are resolved for the VIIRS low light imaging data, making these ideal for moment production and analyses.

We foresee several applications for moment grids constructed for VIIRS night-time lights, such as distinguishing residential from commercial zones within urban centres and tracking the evolution and stability of lighting through time. High levels of skew and kurtosis serve as indicators of grid cells having large numbers of outliers. Negative skew indicates the outliers with radiance levels below the predominant data range and positive skew indicates the prominence of outliers with radiances above the core data range. We believe that having the four moments will provide new avenues for exploring the evolution of electric lighting and the definition of zones within urban centres. With the four moments, it may be possible to define trajectories for lighting growth and the identification of trajectory shifts caused by conversions in lighting types and shielding. It may be possible to visualize these temporal trajectories as the movement of individual grid cells through the moment scattergrams.

Acknowledgment

Multiple sponsors have supported this research over the years, including NOAA, NASA and the Rockefeller Foundation. The authors gratefully acknowledge NASA and NOAA's efforts to build, fly and calibrate the VIIRS data this study relied on.

Disclosure statement

No potential conflict of interest was reported by the authors.

Data access

VNL v.3 DNB temporal profiles: https://eogdata.mines.edu/wwwdata/hidden/dnb_profiles_deliver_licorr/

Moment scattergrams:
https://eogdata.mines.edu/wwwdata/hidden/dnb_moments_scattergrams/

Moment grids:
https://eogdata.mines.edu/wwwdata/hidden/dnb_moments_stats_grids/

References

Elvidge, C. D., K. Baugh, T. Ghosh, M. Zhizhin, F. Chi Hsu, T. Sparks, M. Bazilian, P. C. Sutton, K. Houngbedji, and R. Goldblatt. 2022a. "Fifty Years of Nightly Global Low-Light Imaging Satellite Observations." *Frontiers in Remote Sensing* 3: 79. doi:10.3389/frsen.2022.919937.

Elvidge, C. D., K. E. Baugh, E. A. Kihn, H. W. Kroehl, and E. R. Davis. 1997. "Mapping City Lights with Nighttime Data from the DMSP Operational Linescan System." *Photogrammetric Engineering and Remote Sensing* 63 (6): 727–734.

Elvidge, C. D., K. Baugh, M. Zhizhin, F. Chi Hsu, and T. Ghosh. 2017. "VIIRS Night-Time Lights." *International Journal of Remote Sensing* 38 (21): 5860–5879. doi:10.1080/01431161.2017.1342050.

Elvidge, C. D., T. Ghosh, F.C. Hsu, M. Zhizhin, and M. Bazilian. 2020b. "The Dimming of Lights in China During the COVID-19 Pandemic." *Remote Sensing* 12 (17): 2851. doi:10.3390/rs12172851.

Elvidge, C. D., F.C. Hsu, M. Zhizhin, T. Ghosh, J. Taneja, and M. Bazilian. 2020a. "Indicators of Electric Power Instability from Satellite Observed Nighttime Lights." *Remote Sensing* 12 (19): 3194. doi:10.3390/rs12193194.

Elvidge, C. D., M. Zhizhin, D. Keith, S. D. Miller, F. Chi Hsu, T. Ghosh, S. J. Anderson, et al. 2022b. "The VIIRS Day/Night Band: A Flicker Meter in Space?" *Remote Sensing* 14 (6): 1316.

Fiori, A. M., and M. Zenga. 2009. "Karl Pearson and the Origin of Kurtosis." *International Statistical Review* 77 (1): 40–50. doi:10.1111/j.1751-5823.2009.00076.x.

Ghosh, T., K. E. Baugh, C. D. Elvidge, M. Zhizhin, A. Poyda, and F.C. Hsu. 2021. "Extending the DMSP Nighttime Lights Time Series Beyond 2013." *Remote Sensing* 13 (24): 5004. doi:10.3390/rs13245004.

Hsu, F., M. Zhizhin, T. Ghosh, C. Elvidge, and J. Taneja. 2021. "The Annual Cycling of Nighttime Lights in India." *Remote Sensing* 13 (6): 1199. doi:10.3390/rs13061199.

Krishnamoorthy, K. 2006. *Handbook of Statistical Distributions with Applications*. Chapman and Hall/CRC.

O'Kelly, M. E. 1998. "A Geographer's Analysis of Hub-And-Spoke Networks." *Journal of Transport Geography* 6 (3): 171–186. doi:10.1016/S0966-6923(98)00010-6.

Sattin, F., M. Agostini, R. Cavazzana, G. Serianni, P. Scarin, and N. Vianello. 2009. "About the Parabolic Relation Existing Between the Skewness and the Kurtosis in Time Series of Experimental Data." *Physica Scripta* 79 (4): 045006. doi:10.1088/0031-8949/79/04/045006.